

---

# Residual Stream Analysis with Multi-Layer SAEs

---

Tim Lawson\* Lucy Farnik Conor Houghton Laurence Aitchison  
School of Engineering Mathematics and Technology  
University of Bristol  
Bristol, UK

## Abstract

Sparse autoencoders (SAEs) are a promising approach to interpreting the internal representations of transformer language models. However, standard SAEs are trained separately on each transformer layer, making it difficult to use them to study how information flows across layers. To solve this problem, we introduce the multi-layer SAE (MLSAE): a single SAE trained on the residual stream activation vectors from every transformer layer simultaneously. The residual stream is usually understood as preserving information across layers, so we expected to, and did, find individual SAE features that are active at multiple layers. Interestingly, while a single SAE feature is active at different layers for different prompts, for a single prompt, we find that a single feature is far more likely to be active at a single layer. For larger underlying models, we find that the cosine similarities between adjacent layers in the residual stream are higher, so we expect more features to be active at multiple layers. These results show that MLSAEs are a promising method to study information flow in transformers. We release our code to train and analyze MLSAEs at <https://github.com/tim-lawson/mlsae>.

## 1 Introduction

Sparse autoencoders (SAEs) learn interpretable directions or ‘features’ in the representation spaces of language models (Elhage et al., 2022; Cunningham et al., 2023; Bricken et al., 2023). Typically, SAEs are trained on the activation vectors from a single model layer (Gao et al., 2024; Templeton et al., 2024; Lieberum et al., 2024). This approach illuminates the representations within a layer. However, Olah (2024); Templeton et al. (2024) believe that models may encode meaningful concepts by simultaneous activations in multiple layers, which standard dictionary learning does not address. Furthermore, it is not straightforward to automatically identify correspondences between features from SAEs trained at different layers, which may complicate circuit analysis (Conmy et al., 2023).

To solve this problem, we take inspiration from the residual stream perspective, which states that transformers (Vaswani et al., 2017) selectively write information to and read information from token positions with self-attention and MLP layers (Elhage et al., 2021; Ferrando et al., 2024). The results of subsequent circuit analyses, like the explanation of the indirect object identification task presented by Wang et al. (2022), support this viewpoint and cause us to expect the activation vectors at adjacent layers in the residual stream to be similar.

To capture the structure shared between layers in the residual stream, we introduce the multi-layer SAE (MLSAE): a single SAE trained on the residual stream activation vectors from every layer of a transformer language model. Importantly, the autoencoder itself has a single hidden layer – it is multi-layer only in the sense that it is trained at multiple layers of the underlying transformer. In particular, we consider the activation vectors from each layer as separate training examples, which

---

\*Correspondence to [tim.lawson@bristol.ac.uk](mailto:tim.lawson@bristol.ac.uk).

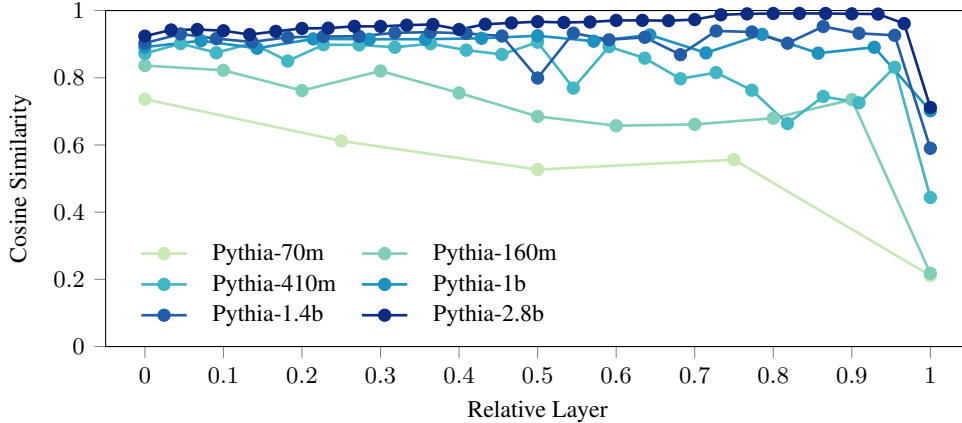


Figure 1: The mean cosine similarities between the residual stream activation vectors at adjacent layers of transformers over the entire training dataset (Gao et al., 2020). The  $x$ -axis is the index of the lower of each pair of adjacent layers, divided by the number of pairs. The error bars show the standard errors in the mean, but are too small to be visible.

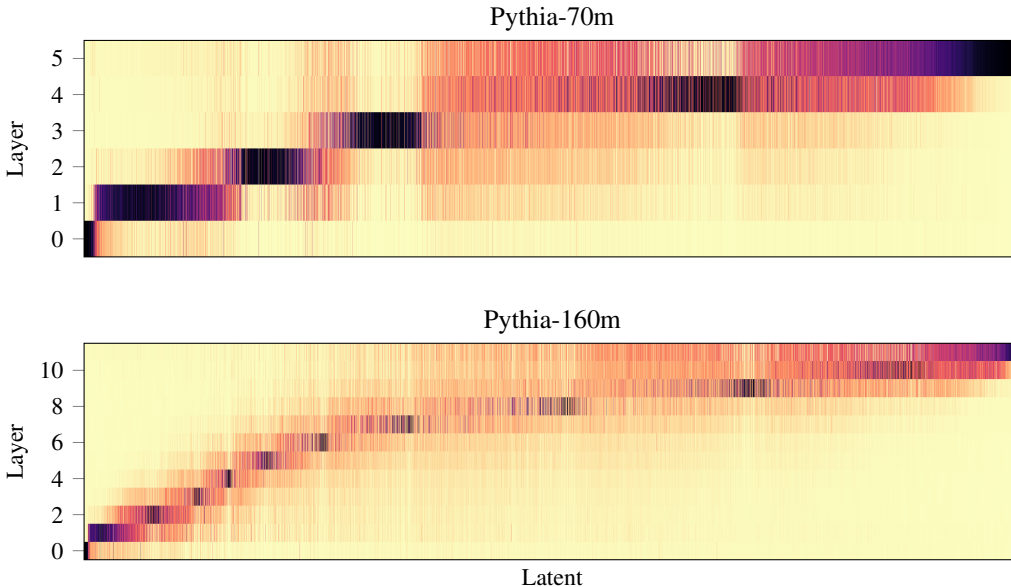


Figure 2: Heatmaps of the distributions of latent activations over layers for MLSAEs trained on Pythia-70m and 160m with an expansion factor of  $R = 64$  and  $k = 32$  over the entire training dataset. The latents are sorted in ascending order of center of mass (Equation 7). We provide similar heatmaps for other expansion factors in the appendix (Figure 10).

is equivalent to training a single SAE at each layer individually but with the parameters tied across layers. We briefly discuss alternative methods in Section 5.

We show that multi-layer SAEs achieve comparable reconstruction error and downstream loss to single-layer SAEs (Appendix B) while allowing us to directly identify and analyze features that are active at multiple layers. In aggregate, we find many features shared between layers, but for individual prompts, most features are active at only a single layer of a small transformer. This suggests that feature activations are more layer-specific in more specific contexts. For larger transformers, we show that the residual stream activation vectors at adjacent layers are more similar (from Pythia-70m to 2.8b), and more features are shared between layers with the same hyperparameters (Pythia-70m and 160m only). Therefore, we speculate that the smaller the changes to the residual stream by each transformer block, the more multi-layer features MLSAEs can learn.

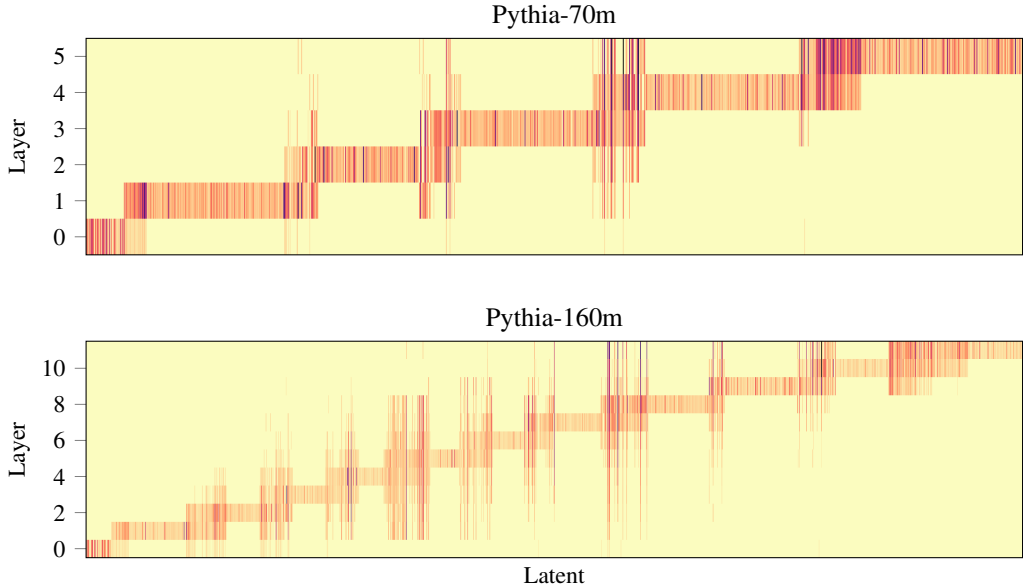


Figure 3: Heatmaps of the maximum latent activations for MLSAEs trained on Pythia-70m and 160m with an expansion factor of  $R = 64$  and  $k = 32$ , given the prompt “When John and Mary went to the store, John gave” (Wang et al., 2022). We take the maximum activation over the tokens in the prompt, exclude latents with maximum activation below  $1 \times 10^{-3}$ , and sort them in ascending order of center of mass over the prompt. We provide similar heatmaps for other prompts in the appendix (Figure 12).

## 2 Related work

A sparse code represents many signals, such as sensory inputs, by simultaneously activating a relatively small number of elements, such as neurons (Olshausen and Field, 1996; Bell and Sejnowski, 1997). Sparse dictionary learning (SDL) approximates a set of input vectors by linear combinations of a relatively small number of learned basis vectors. The learned basis is usually overcomplete: it has a greater dimension than the inputs. SDL algorithms include Independent Component Analysis (Bell and Sejnowski, 1995; Hyvärinen and Oja, 2000; Le et al., 2011) and sparse autoencoders (Lee et al., 2006; Ng, 2011; Makhzani and Frey, 2014).

The activations of language models have been hypothesized to be a dense, compressed version of a sparse, expanded representation space (Elhage et al., 2021, 2022). Under this view, there are interpretable directions in the dense representation spaces corresponding to distinct semantic concepts, whereas their basis vectors (neurons) are ‘polysemantic’ (Park et al., 2023; Wattenberg and Viégas, 2024). It has been shown theoretically (Wright and Ma, 2022) and empirically (Elhage et al., 2022; Sharkey et al., 2022; Whittington et al., 2023) that SDL recovers ground-truth features in toy models, and that learned dictionary elements are more interpretable than the basis vectors of language models (Cunningham et al., 2023; Bricken et al., 2023).

The standard SAE architecture is a single hidden layer with a ReLU activation function and an  $L^1$  sparsity penalty in the training loss (Bricken et al., 2023), but various activation functions (Makhzani and Frey, 2014; Konda et al., 2015; Rajamanoharan et al., 2024b,a) and objectives (Braun et al., 2024) have been proposed. The prevailing approach is to train an SAE on the activation vectors from a single transformer layer, except for Kissane et al. (2024), who concatenate the outputs of multiple attention heads in a single layer, and Yun et al. (2021), who learn an undercomplete basis for the residual stream at multiple layers, albeit by iterative optimization instead of with an autoencoder.

Mechanistic interpretability research often attempts to identify circuits: computational subgraphs of neural networks that implement specific behaviors (Olah et al., 2020; Wang et al., 2022; Conmy et al., 2023; Dunefsky et al., 2024; García-Carrasco et al., 2024; Marks et al., 2024). Representing networks in terms of SAE features may help to improve circuit discovery (He et al., 2024; O’Neill and Bui, 2024), and features can be used to construct steering vectors (Subramani et al., 2022; Templeton

et al., 2024; Makelov, 2024). Importantly, SAEs can be scaled up to the activations of large language models, where we expect the number of distinct semantic concepts to be extremely large (Templeton et al., 2024; Gao et al., 2024; Lieberum et al., 2024).

The key difference between previous work in the SAE literature (Bricken et al., 2023; Cunningham et al., 2023; Templeton et al., 2024; Gao et al., 2024) and our work is that we introduce the multi-layer SAE, i.e. we train a single SAE at all layers of the residual stream.

### 3 Methods

The key idea with a multi-layer SAE is to train a single SAE on the residual stream activation vectors from every layer. In particular, we consider the activations at each layer as different training examples. Hence, for residual stream activation vectors of model dimension  $d$ , the inputs to the multi-layer SAE also have dimension  $d$ . We use the terms ‘SAE feature’ and ‘latent’ interchangeably.

We train MLSAEs on GPT-style language models from the Pythia suite (Biderman et al., 2023). We are primarily interested in the computation performed by self-attention and MLP layers on intermediate representations (Valeriani et al., 2023), so we exclude the input embeddings before the first transformer block and take the last-layer activations before the final layer norm.

We use a  $k$ -sparse autoencoder (Makhzani and Frey, 2014; Gao et al., 2024), which directly controls the sparsity of the latent space by introducing a TopK activation function that keeps only the  $k$  largest latents. The  $k$  largest latents are almost always positive for  $k \ll d$ , but we follow Gao et al. (2024) in applying a ReLU activation function to guarantee non-negativity. This setup effectively fixes the sparsity ( $L^0$  norm) of the latents at  $k$  per activation vector (layer and token) throughout training. For input vectors  $\mathbf{x} \in \mathbb{R}^d$  and latent vectors  $\mathbf{h} \in \mathbb{R}^n$ , the encoder and decoder are defined by:

$$\mathbf{h} = \text{ReLU}(\text{TopK}(\mathbf{W}_{\text{enc}}\mathbf{x} - \mathbf{b}_{\text{pre}})) \quad (1)$$

$$\hat{\mathbf{x}} = \mathbf{W}_{\text{dec}}\mathbf{h} + \mathbf{b}_{\text{pre}} \quad (2)$$

where  $\mathbf{W}_{\text{enc}} \in \mathbb{R}^{n \times d}$ ,  $\mathbf{W}_{\text{dec}} \in \mathbb{R}^{d \times n}$ , and  $\mathbf{b}_{\text{pre}} \in \mathbb{R}^d$ . We constrain the pre-encoder bias  $\mathbf{b}_{\text{pre}}$  to be the negative of the post-decoder bias, following Bricken et al. (2023); Gao et al. (2024).

Like Gao et al. (2024), we standardize activation vectors to zero mean and unit variance before passing them to the autoencoder. However, we use the fraction of variance unexplained (FVU) instead of the mean squared error (MSE) as the reconstruction error to handle differences in the variances of the inputs from each layer. We include an auxiliary loss term that models the MSE reconstruction error using the  $k_{\text{aux}}$  largest dead latents (Gao et al., 2024, Appendix A.2). Following Bricken et al. (2023); Cunningham et al. (2023), we consider latents ‘dead’ if they have not activated within the last 10 million tokens (for inputs from any layer). Hence, the full loss is:

$$\mathcal{L} = \text{FVU}(\mathbf{x}, \hat{\mathbf{x}}) + \alpha \|\mathbf{e} - \hat{\mathbf{e}}\|_2^2 \quad (3)$$

$$\text{FVU}(\mathbf{x}, \hat{\mathbf{x}}) = \frac{1}{L} \sum_{\ell=0}^L \frac{\|\mathbf{x}_\ell - \hat{\mathbf{x}}_\ell\|_2^2}{\text{Var}(\mathbf{x}_\ell)} \quad (4)$$

Gao et al. (2024) propose the auxiliary loss term as a means to reduce the number of dead latents, where  $\alpha$  is a small coefficient,  $\mathbf{e} = \|\mathbf{x} - \hat{\mathbf{x}}\|_2^2$  is the MSE reconstruction error of the main model, and  $\hat{\mathbf{e}}$  is the reconstruction using the top- $k_{\text{aux}}$  dead latents:

$$\mathbf{h}_{\text{dead}} = \text{ReLU}(\text{TopK}_{\text{aux}}(\text{Dead}(\mathbf{W}_{\text{enc}}\mathbf{x} - \mathbf{b}_{\text{pre}}))) \quad (5)$$

$$\hat{\mathbf{e}} = \mathbf{W}_{\text{dec}}\mathbf{h}_{\text{dead}} + \mathbf{b}_{\text{pre}} \quad (6)$$

Here, Dead keeps only the dead latents. Following Gao et al. (2024), we choose  $k_{\text{aux}}$  as a power of 2 close to  $d/2$  and  $\alpha = 1/32$ . The implementation is based on Gao et al. (2023); Belrose (2024); we provide further details in Appendix A.

Our hyperparameters are the expansion factor  $R = n/d$ , the ratio between the model dimension and the number of latents, and  $k$ , the number of largest latents to keep in the TopK activation function. We choose expansion factors as powers of 2 between 1 and 256, yielding autoencoders with between 512 and 131072 latents for Pythia-70m, and  $k$  as powers of 2 between 16 and 512.

## 4 Results

Guided by the residual stream perspective (Elhage et al., 2021; Ferrando et al., 2024), we expected dense activation vectors to be relatively similar across layers. As an approximate measure of the degree to which information is preserved in the residual stream, we computed the cosine similarities between the activation vectors at adjacent layers. A similarity of one means that the information represented at a token position is unchanged by the intervening residual block, whereas a similarity of zero means the activation vectors on either side of the block are orthogonal. We had expected changes in the residual stream to become smaller as the model size increased, and we confirmed that the cosine similarities increased accordingly (Figure 1).

Given that residual stream activations are similar across layers (or have high cosine similarity), we expected to find many MLSAE features that are active at multiple layers. We confirmed this prediction over the training dataset of 1 billion tokens (Figure 2). Interestingly, we found that for individual prompts, a much greater proportion of latents are active at only a single layer (Figure 3).

To understand whether latents are specific to single layers or shared between layers, we computed the distribution over layers for each latent  $p_i(\ell)$ , where  $i \in 0, \dots, n - 1$  is the latent index and  $\ell \in 0, \dots, L - 1$  is the layer index. The probability under this distribution is proportional to the total activation of the latent at that layer, aggregating over inputs:

$$p_i(\ell) = \frac{\sum_{\alpha} h_i(\mathbf{x}_{\alpha, \ell})}{\sum_{\alpha} \sum_{\ell=0}^L h_i(\mathbf{x}_{\alpha, \ell})} \quad (7)$$

Here,  $\mathbf{x}_{\alpha, \ell}$  is the dense activation vector at token position  $\alpha$  and layer  $\ell$ , while  $h_i(\mathbf{x}_{\alpha, \ell})$  is the activation of the  $i$ -th autoencoder latent at that token position and layer. Given this distribution, we can compute its expected value (the center of mass) and standard deviation. We use the center of mass to order the latents in Figures 2 and 3.

The standard deviation of the distribution over layers measures the degree to which features are active at a single layer (in which case, the standard deviation is zero) versus multiple layers (in which case, it is positive). Hence, we considered the dependence of the standard deviation of this value (i.e. the degree to which features are shared between layers) on the expansion factor (Figure 4). We found that the standard deviation was remarkably similar for different expansion factors: it changes by less than a factor of  $1/2$ , while the expansion factor changes by more than two orders of magnitude. Furthermore, the direction of the change is not systematic: it decreases slightly as the expansion factor increases, except at the largest value, where it increases. This is difficult to interpret, except to state that the extent of multi-layer features is remarkably robust to the choice of expansion factor.

## 5 Discussion

We introduced the multi-layer SAE (MLSAE), where we train a single SAE on the activations at every layer of the residual stream. This allowed us to study not only how information is represented within a single transformer layer but also how information flows through the residual stream.

By looking at cosine similarities, we confirmed that residual stream activations are relatively similar across layers. We then considered the activations of MLSAE features at different layers. When aggregating over 1 billion tokens, we found many features active at multiple layers. However, for specific prompts, we found more features active at only a single layer. Finally, we found that the degree to which features were shared between layers was remarkably robust to changes in the expansion factor (a change of more than two orders of magnitude produced a change by a factor of less than  $1/2$  in the mean standard deviation).

An alternative approach to studying cross-layer behavior is to concatenate activation vectors from multiple layers into a single vector of length  $d \times L$ , where  $d$  is the model dimension and  $L$  is the number of layers, to form the input to a single SAE. This method is analogous to Kissane et al. (2024), except that they concatenate activations from different attention heads within a single layer, while we are concerned with activations from different layers of the residual stream. In fact, we started by pursuing this approach: the difference from our proposal is that MLSAEs take inputs of length  $d$ , and we treat activations from different layers as different training examples. We made this change because it allows us to compute the SAE feature activations at multiple layers from the underlying dense

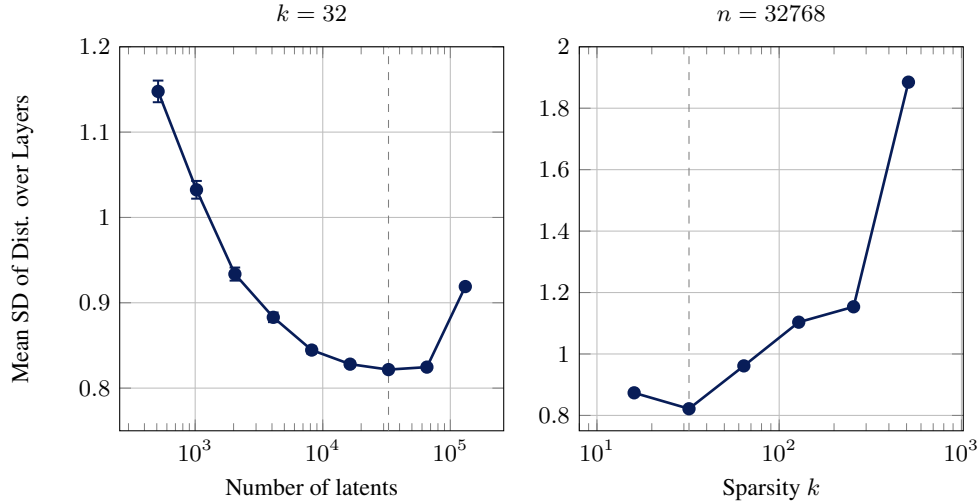


Figure 4: The mean of the standard deviations in the latent distributions over layers (Equation 7) for MLSAEs trained on Pythia-70m with  $k = 32$  over the entire training dataset. The error bars show the standard errors in the mean.

activations and to compare them (e.g. to see which features ‘appear’ or disappear). The concatenated approach would not allow this because it takes inputs from all layers simultaneously and produces a single vector that jointly describes the activations at all layers. While this might capture ‘cross-layer superposition,’ which we take to mean a small number of simultaneously active sparse features at multiple layers encoding a single meaningful concept (Olah, 2024; Templeton et al., 2024), it is unclear how one would use it to understand the flow of information through a transformer.

In this paper, we assumed that the sparse basis was the same at every layer in the residual stream. Relaxing this assumption by allowing small changes in the basis between layers could improve performance, but we leave this to future work. It also remains to investigate whether our observations generalize to larger models. Notably, we showed that the cosine similarities between adjacent layers increase in models from 70m to 2.8b parameters, so we expect our approach to become increasingly useful. However, due to time constraints, we have only trained MLSAEs on Pythia-70m and 160m.

Finally, we believe that understanding information flow in transformers is critical to identifying meaningful circuits and that the MLSAE, or future approaches based on it, may prove an important building block for these methods.

## References

A. J. Bell and T. J. Sejnowski. An Information-Maximization Approach to Blind Separation and Blind Deconvolution. *Neural Computation*, 7(6):1129–1159, Nov. 1995. ISSN 0899-7667. doi: 10.1162/neco.1995.7.6.1129. URL <https://ieeexplore.ieee.org/abstract/document/6796129>. Conference Name: Neural Computation.

A. J. Bell and T. J. Sejnowski. The “independent components” of natural scenes are edge filters. *Vision Research*, 37(23):3327–3338, Dec. 1997. ISSN 0042-6989. doi: 10.1016/S0042-6989(97)00121-1. URL <https://www.sciencedirect.com/science/article/pii/S0042698997001211>.

N. Belrose. EleutherAI/sae, May 2024. URL <https://github.com/EleutherAI/sae>.

S. Biderman, H. Schoelkopf, Q. G. Anthony, H. Bradley, K. O’Brien, E. Hallahan, M. A. Khan, S. Purohit, U. S. Prashanth, E. Raff, A. Skowron, L. Sutawika, and O. V. D. Wal. Pythia: A Suite for Analyzing Large Language Models Across Training and Scaling. In *Proceedings of the 40th International Conference on Machine Learning*, pages 2397–2430. PMLR, July 2023. URL <https://proceedings.mlr.press/v202/biderman23a.html>. ISSN: 2640-3498.

- D. Braun, J. Taylor, N. Goldowsky-Dill, and L. Sharkey. Identifying Functionally Important Features with End-to-End Sparse Dictionary Learning, May 2024. URL <http://arxiv.org/abs/2405.12241>. arXiv:2405.12241 [cs].
- T. Bricken, A. Templeton, J. Batson, B. Chen, A. Jermyn, T. Conerly, N. Turner, C. Anil, C. Denison, and A. Askell. Towards Monosemanticity: Decomposing Language Models With Dictionary Learning, 2023. URL <https://transformer-circuits.pub/2023/monosemantic-features>.
- A. Conmy, A. Mavor-Parker, A. Lynch, S. Heimersheim, and A. Garriga-Alonso. Towards Automated Circuit Discovery for Mechanistic Interpretability. *Advances in Neural Information Processing Systems*, 36:16318–16352, Dec. 2023. URL [https://proceedings.neurips.cc/paper\\_files/paper/2023/hash/34e1dbe95d34d7ebaf99b9bcaeb5b2be-Abstract-Conference.html](https://proceedings.neurips.cc/paper_files/paper/2023/hash/34e1dbe95d34d7ebaf99b9bcaeb5b2be-Abstract-Conference.html).
- H. Cunningham, A. Ewart, L. Riggs, R. Huben, and L. Sharkey. Sparse Autoencoders Find Highly Interpretable Features in Language Models, Oct. 2023. URL <http://arxiv.org/abs/2309.08600>. arXiv:2309.08600 [cs].
- J. Dunefsky, P. Chlenski, and N. Nanda. Transcoders Find Interpretable LLM Feature Circuits, June 2024. URL <http://arxiv.org/abs/2406.11944>. arXiv:2406.11944 [cs].
- N. Elhage, N. Nanda, C. Olsson, T. Henighan, N. Joseph, B. Mann, A. Askell, Y. Bai, A. Chen, and T. Conerly. A Mathematical Framework for Transformer Circuits, 2021. URL <https://transformer-circuits.pub/2021/framework/index.html>.
- N. Elhage, T. Hume, C. Olsson, N. Schiefer, T. Henighan, S. Kravec, Z. Hatfield-Dodds, R. Lasenby, D. Drain, C. Chen, R. Grosse, S. McCandlish, J. Kaplan, D. Amodei, M. Wattenberg, and C. Olah. Toy Models of Superposition, Sept. 2022. URL <http://arxiv.org/abs/2209.10652>. arXiv:2209.10652 [cs].
- J. Ferrando, G. Sarti, A. Bisazza, and M. R. Costa-jussà. A Primer on the Inner Workings of Transformer-based Language Models, May 2024. URL <http://arxiv.org/abs/2405.00208>. arXiv:2405.00208 [cs].
- L. Gao, S. Biderman, S. Black, L. Golding, T. Hoppe, C. Foster, J. Phang, H. He, A. Thite, N. Nabeshima, S. Presser, and C. Leahy. The Pile: An 800GB Dataset of Diverse Text for Language Modeling, Dec. 2020. URL <http://arxiv.org/abs/2101.00027>. arXiv:2101.00027 [cs].
- L. Gao, T. D. la Tour, and J. Wu. `openai/sparse_autoencoder`, Dec. 2023. URL [https://github.com/openai/sparse\\_autoencoder](https://github.com/openai/sparse_autoencoder).
- L. Gao, T. D. la Tour, H. Tillman, G. Goh, R. Troll, A. Radford, I. Sutskever, J. Leike, and J. Wu. Scaling and evaluating sparse autoencoders, June 2024. URL <http://arxiv.org/abs/2406.04093>. arXiv:2406.04093 [cs].
- J. García-Carrasco, A. Maté, and J. C. Trujillo. How does GPT-2 Predict Acronyms? Extracting and Understanding a Circuit via Mechanistic Interpretability. In *Proceedings of The 27th International Conference on Artificial Intelligence and Statistics*, pages 3322–3330. PMLR, Apr. 2024. URL <https://proceedings.mlr.press/v238/garcia-carrasco24a.html>. ISSN: 2640-3498.
- Z. He, X. Ge, Q. Tang, T. Sun, Q. Cheng, and X. Qiu. Dictionary Learning Improves Patch-Free Circuit Discovery in Mechanistic Interpretability: A Case Study on Othello-GPT, Feb. 2024. URL <http://arxiv.org/abs/2402.12201>. arXiv:2402.12201 [cs].
- D. Hendrycks, C. Burns, S. Basart, A. Zou, M. Mazeika, D. Song, and J. Steinhardt. Measuring Massive Multitask Language Understanding, Jan. 2021. URL <http://arxiv.org/abs/2009.03300>. arXiv:2009.03300 [cs].
- A. Hyvärinen and E. Oja. Independent component analysis: algorithms and applications. *Neural Networks*, 13(4):411–430, June 2000. ISSN 0893-6080. doi: 10.1016/S0893-6080(00)00026-5. URL <https://www.sciencedirect.com/science/article/pii/S0893608000000265>.
- D. P. Kingma and J. Ba. Adam: A Method for Stochastic Optimization, Jan. 2017. URL <http://arxiv.org/abs/1412.6980>. arXiv:1412.6980 [cs].

- C. Kissane, R. Krzyzanowski, J. I. Bloom, A. Conmy, and N. Nanda. Interpreting Attention Layer Outputs with Sparse Autoencoders. June 2024. URL <https://openreview.net/forum?id=fewUBDwjji>.
- K. Konda, R. Memisevic, and D. Krueger. Zero-bias autoencoders and the benefits of co-adapting features, Apr. 2015. URL <http://arxiv.org/abs/1402.3337>. arXiv:1402.3337 [cs, stat].
- Q. Le, A. Karpenko, J. Ngiam, and A. Ng. ICA with Reconstruction Cost for Efficient Overcomplete Feature Learning. In *Advances in Neural Information Processing Systems*, volume 24. Curran Associates, Inc., 2011. URL <https://proceedings.neurips.cc/paper/2011/hash/233509073ed3432027d48b1a83f5fbd2-Abstract.html>.
- H. Lee, A. Battle, R. Raina, and A. Ng. Efficient sparse coding algorithms. In *Advances in Neural Information Processing Systems*, volume 19. MIT Press, 2006. URL [https://proceedings.neurips.cc/paper\\_files/paper/2006/hash/2d71b2ae158c7c5912cc0bbde2bb9d95-Abstract.html](https://proceedings.neurips.cc/paper_files/paper/2006/hash/2d71b2ae158c7c5912cc0bbde2bb9d95-Abstract.html).
- T. Lieberum, S. Rajamanoharan, A. Conmy, L. Smith, N. Sonnerat, V. Varma, J. Kramár, A. Dragan, R. Shah, and N. Nanda. Gemma Scope: Open Sparse Autoencoders Everywhere All At Once on Gemma 2, Aug. 2024. URL <http://arxiv.org/abs/2408.05147>. arXiv:2408.05147 [cs].
- A. Makelov. Sparse Autoencoders Match Supervised Features for Model Steering on the IOI Task. June 2024. URL <https://openreview.net/forum?id=JdrVuEQih5>.
- A. Makhzani and B. Frey. k-Sparse Autoencoders, Mar. 2014. URL <http://arxiv.org/abs/1312.5663>. arXiv:1312.5663 [cs].
- S. Marks, C. Rager, E. J. Michaud, Y. Belinkov, D. Bau, and A. Mueller. Sparse Feature Circuits: Discovering and Editing Interpretable Causal Graphs in Language Models, Mar. 2024. URL <http://arxiv.org/abs/2403.19647>. arXiv:2403.19647 [cs].
- A. Ng. Sparse autoencoder, 2011. URL <https://graphics.stanford.edu/courses/cs233-21-spring/ReferencedPapers/SAE.pdf>.
- C. Olah. The Next Five Hurdles, July 2024. URL <https://transformer-circuits.pub/2024/july-update/index.html#hurdles>.
- C. Olah, N. Cammarata, L. Schubert, G. Goh, M. Petrov, and S. Carter. Zoom In: An Introduction to Circuits. *Distill*, 5(3), Mar. 2020. ISSN 2476-0757. doi: 10.23915/distill.00024.001. URL <https://distill.pub/2020/circuits/zoom-in>.
- B. A. Olshausen and D. J. Field. Emergence of simple-cell receptive field properties by learning a sparse code for natural images. *Nature*, 381(6583):607–609, June 1996. ISSN 1476-4687. doi: 10.1038/381607a0. URL <https://www.nature.com/articles/381607a0>. Publisher: Nature Publishing Group.
- C. O’Neill and T. Bui. Sparse Autoencoders Enable Scalable and Reliable Circuit Identification in Language Models, May 2024. URL <http://arxiv.org/abs/2405.12522>. arXiv:2405.12522 [cs].
- K. Park, Y. J. Choe, and V. Veitch. The Linear Representation Hypothesis and the Geometry of Large Language Models, Nov. 2023. URL <http://arxiv.org/abs/2311.03658>. arXiv:2311.03658 [cs, stat].
- S. Rajamanoharan, A. Conmy, L. Smith, T. Lieberum, V. Varma, J. Kramar, R. Shah, and N. Nanda. Improving Sparse Decomposition of Language Model Activations with Gated Sparse Autoencoders. June 2024a. URL <https://openreview.net/forum?id=Ppj5KvzU8Q>.
- S. Rajamanoharan, T. Lieberum, N. Sonnerat, A. Conmy, V. Varma, J. Kramár, and N. Nanda. Jumping Ahead: Improving Reconstruction Fidelity with JumpReLU Sparse Autoencoders, July 2024b. URL <http://arxiv.org/abs/2407.14435>. arXiv:2407.14435 [cs].
- L. Sharkey, D. Braun, and B. Millidge. Taking features out of superposition with sparse autoencoders, Dec. 2022. URL <https://www.alignmentforum.org/posts/z6QQJbtpkEAX3Aojj/interim-research-report-taking-features-out-of-superposition>.



- N. Subramani, N. Suresh, and M. Peters. Extracting Latent Steering Vectors from Pretrained Language Models. In S. Muresan, P. Nakov, and A. Villavicencio, editors, *Findings of the Association for Computational Linguistics: ACL 2022*, pages 566–581, Dublin, Ireland, May 2022. Association for Computational Linguistics. doi: 10.18653/v1/2022.findings-acl.48. URL <https://aclanthology.org/2022.findings-acl.48>.
- A. Templeton, T. Conerly, J. Marcus, J. Lindsey, T. Bricken, B. Chen, A. Pearce, C. Citro, E. Ameisen, A. Jones, H. Cunningham, N. L. Turner, C. McDougall, M. MacDiarmid, A. Tamkin, E. Durmus, T. Hume, F. Mosconi, C. D. Freeman, T. R. Sumers, E. Rees, J. Batson, A. Jermyn, S. Carter, C. Olah, and T. Henighan. Scaling Monosemanticity: Extracting Interpretable Features from Claude 3 Sonnet, May 2024. URL <https://transformer-circuits.pub/2024/scaling-monosemanticity/index.html>.
- L. Valeriani, D. Doimo, F. Cuturello, A. Laio, A. Ansuini, and A. Cazzaniga. The geometry of hidden representations of large transformer models. *Advances in Neural Information Processing Systems*, 36:51234–51252, Dec. 2023. URL [https://proceedings.neurips.cc/paper\\_files/paper/2023/hash/a0e66093d7168b40246af1cddc025daa-Abstract-Conference.html](https://proceedings.neurips.cc/paper_files/paper/2023/hash/a0e66093d7168b40246af1cddc025daa-Abstract-Conference.html).
- A. Vaswani, N. Shazeer, N. Parmar, J. Uszkoreit, L. Jones, A. N. Gomez, L. Kaiser, and I. Polosukhin. Attention is All you Need. In *Advances in Neural Information Processing Systems*, volume 30. Curran Associates, Inc., 2017. URL [https://papers.nips.cc/paper\\_files/paper/2017/hash/3f5ee243547dee91fbd053c1c4a845aa-Abstract.html](https://papers.nips.cc/paper_files/paper/2017/hash/3f5ee243547dee91fbd053c1c4a845aa-Abstract.html).
- K. Wang, A. Variengien, A. Conmy, B. Shlegeris, and J. Steinhardt. Interpretability in the Wild: a Circuit for Indirect Object Identification in GPT-2 small, Nov. 2022. URL <http://arxiv.org/abs/2211.00593>. arXiv:2211.00593 [cs].
- M. Wattenberg and F. Viégas. Relational Composition in Neural Networks: A Survey and Call to Action. June 2024. URL <https://openreview.net/forum?id=zzCEiUIPk9>.
- J. C. R. Whittington, W. Dorrell, S. Ganguli, and T. E. J. Behrens. Disentanglement with Biological Constraints: A Theory of Functional Cell Types, Mar. 2023. URL <http://arxiv.org/abs/2210.01768>. arXiv:2210.01768 [cs, q-bio].
- J. Wright and Y. Ma. *High-Dimensional Data Analysis with Low-Dimensional Models: Principles, Computation, and Applications*. Cambridge University Press, 1 edition, Jan. 2022. ISBN 978-1-108-77930-2 978-1-108-48973-7. doi: 10.1017/9781108779302. URL <https://www.cambridge.org/highereducation/product/9781108779302/book>.
- Z. Yun, Y. Chen, B. Olshausen, and Y. LeCun. Transformer visualization via dictionary learning: contextualized embedding as a linear superposition of transformer factors. In E. Agirre, M. Apidianaki, and I. Vulić, editors, *Proceedings of Deep Learning Inside Out (DeeLIO): The 2nd Workshop on Knowledge Extraction and Integration for Deep Learning Architectures*, pages 1–10, Online, June 2021. Association for Computational Linguistics. doi: 10.18653/v1/2021.deelio-1.1. URL <https://aclanthology.org/2021.deelio-1.1>.

## A Training

We train each autoencoder on 1 billion tokens from the Pile (Gao et al., 2020), excluding the copyrighted Books3 dataset, for a single epoch. Specifically, we concatenate a batch of 1024 text samples with the end-of-sentence token, tokenize the concatenated text, and divide the output into sequences of 2048 tokens, discarding the final incomplete sequence. We use an effective batch size of 131072 tokens (64 sequences) for all experiments.

We do not compute activation vectors and cache them to disk before training, which minimizes storage overhead at the expense of repeated computation. Following Lieberum et al. (2024), we exclude activation vectors corresponding to special tokens (end-of-sentence, beginning-of-sentence, and padding) from the inputs to the autoencoder. The total number of activation vectors is the number of non-special tokens multiplied by the number of layers.

Following the optimization guidelines in Bricken et al. (2023); Gao et al. (2024), we initialize the pre-encoder bias  $\mathbf{b}_{\text{pre}}$  to the geometric median of the first training batch; we initialize the decoder

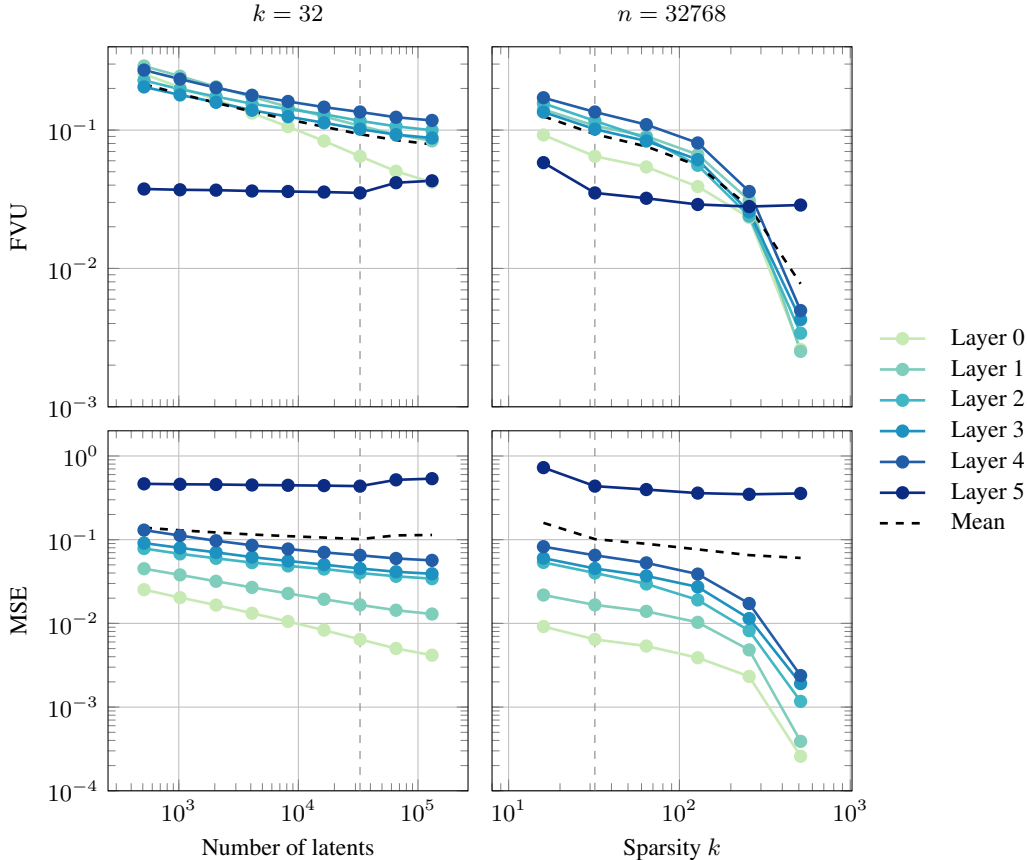


Figure 5: For Pythia-70m and  $k = 32$  (left), the FVU and MSE generally decrease as the expansion factor increases. For inputs from the last layer, we observe instability at the largest expansion factors, which we attribute to fluctuations in the percentage of dead latents (Figure 8). With  $n = 32768$  (right), the FVU and MSE decrease as the sparsity  $k$  increases. While all inputs are standardized before passing them to the encoder, the decoder outputs are rescaled. Hence, the MSE increases across layers because it is not divided by the variance of the inputs.

weight matrix  $\mathbf{W}_{\text{dec}}$  to the transpose of the encoder  $\mathbf{W}_{\text{enc}}$ ; we scale the decoder weight vectors to unit norm at initialization and after each training step; and we remove the component of the gradient of the decoder weight matrix parallel to its weight vectors after each training step.

We use the Adam optimizer (Kingma and Ba, 2017) with the default  $\beta$  parameters, a constant learning rate of  $1 \times 10^{-4}$ , and  $\epsilon = 6.25 \times 10^{-10}$ . Unlike Gao et al. (2024), we do not use gradient clipping or weight averaging, and we use FP16 mixed precision to reduce memory use.

## B Evaluation

### B.1 Reconstruction error and sparsity

While we use the FVU instead of MSE as the reconstruction error in the training loss, we record both metrics for the inputs from each transformer layer and the mean over all layers (Figure 5). The  $L^0$  norm of the latents is fixed at  $k$  per activation vector (layer and token), but we record the  $L^1$  norm (Figure 6). We report the values of these metrics over the first million tokens after training.

For Pythia-70m, the FVU at each layer is comparable to Marks et al. (2024, p. 21), who trained separate SAEs with  $n = 32768$  and  $L^0$  norms between 54 and 108. This is corroborated for the FVU by Cunningham et al. (2023, p. 13) on Pythia-70m, and Gao et al. (2024) for the normalized MSE on layer 8 of GPT-2 small (approximately equivalent to Pythia-160m).

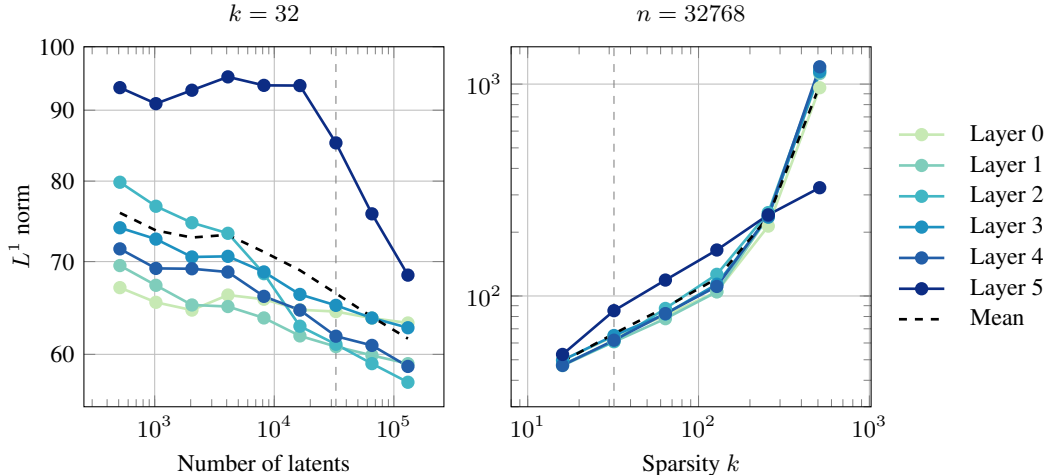


Figure 6: For Pythia-70m and  $k = 32$  (left), the  $L^1$  norm per token (the sum of absolute activations) generally decreases as the number of latents increases. With  $n = 32768$  (right), it increases as the sparsity  $k$  increases. The  $L^0$  norm per token (the count of non-zero activations) is fixed at  $k$ .

## B.2 Downstream loss

The reconstruction error is a proxy for the degree to which an autoencoder explains the behavior of the underlying transformer. Hence, we also measure the change in transformer outputs when the residual stream activations at a given layer are replaced by their reconstruction. Following Braun et al. (2024); Gao et al. (2024); Lieberum et al. (2024), we record the increase in cross-entropy (CE) loss and the Kullback-Leibler (KL) divergence between probability distributions (Figure 7). We report the values of these metrics over the first million tokens after training.

The increase in cross-entropy loss is comparable to Marks et al. (2024, p. 21) for Pythia-70m, Gao et al. (2024, p. 5) and Braun et al. (2024) for GPT-2 small, and Lieberum et al. (2024, p. 7-8) for layer 20 of Gemma 2 2B and 9B.

## B.3 Mean max cosine similarity

Sharkey et al. (2022) define the Mean Max Cosine Similarity (MMCS) between a learned dictionary  $X$  and a ground-truth dictionary  $X'$ . There is no ground-truth dictionary for language models, so a larger learned dictionary or the  $k$  nearest neighbors to each dictionary element are commonly used.

$$\text{MMCS}(X, X') = \frac{1}{|X|} \sum_{\mathbf{x} \in X} \max_{\mathbf{x}' \in X'} \cos \text{sim}(\mathbf{x}, \mathbf{x}') \quad (8)$$

The MMCS serves as a proxy measure for ‘feature splitting’ (Bricken et al., 2023; Braun et al., 2024): as the number of features increases, we expect the decoder weight vectors to be more similar to their nearest neighbors. We compute the MMCS with  $k = 1$  after training (Figure 9).

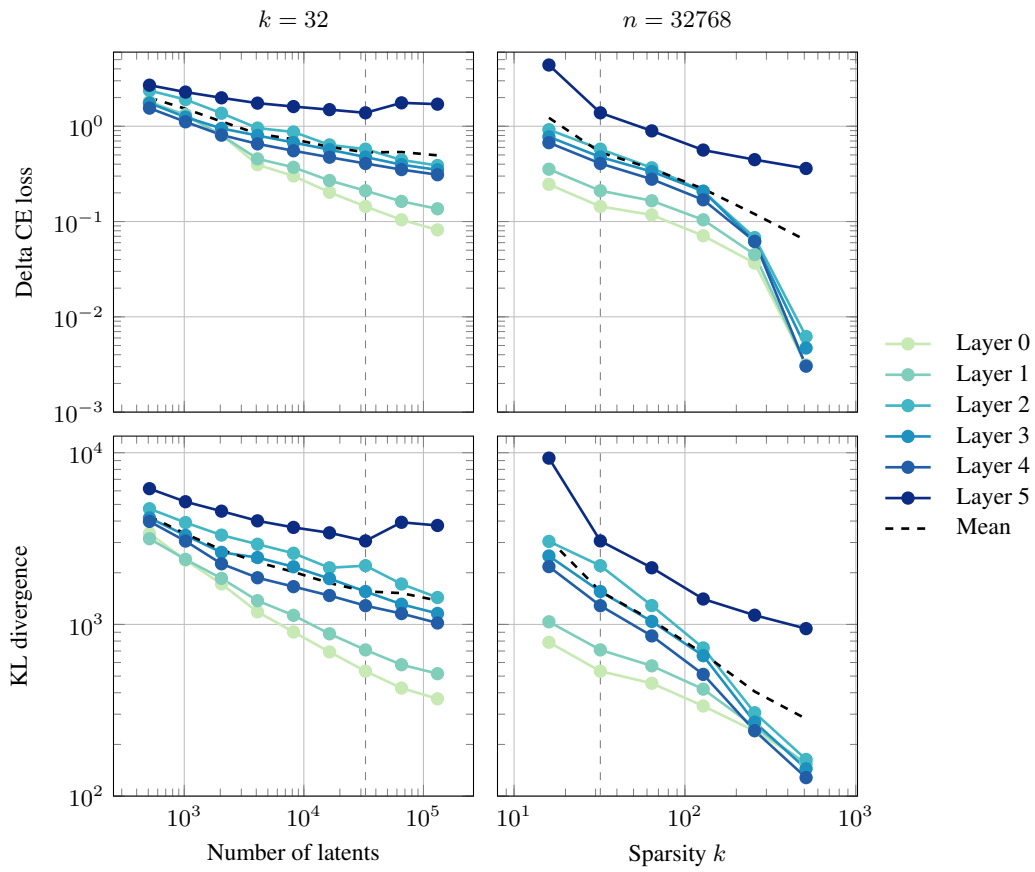


Figure 7: For Pythia-70m and  $k = 32$  (left), the delta CE loss and KL divergence generally decrease as the expansion factor increases, except for inputs from the last layer. With  $n = 32768$  (right), both metrics decrease as the sparsity  $k$  increases, similarly to the FVU and MSE (Figure 5).

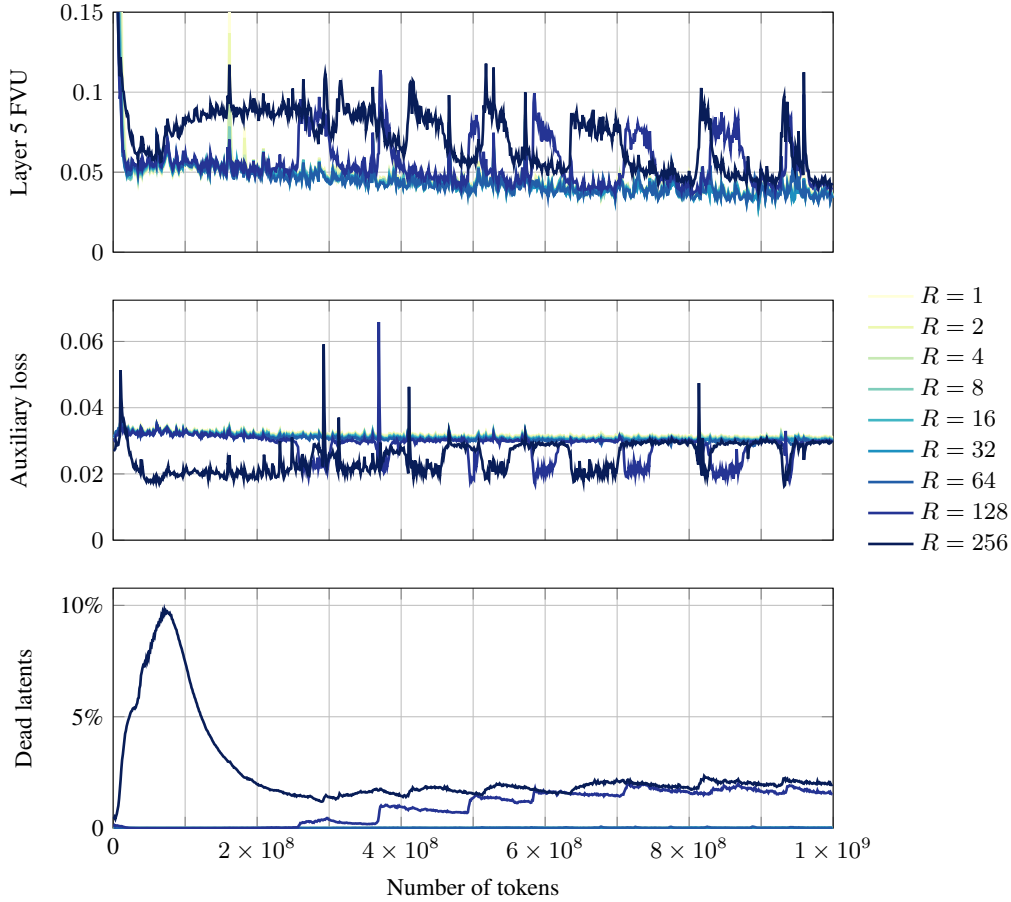


Figure 8: An illustration of the FVU for inputs from the last layer, compared to the auxiliary loss and percentage of dead latents, for MLSAEs trained on Pythia-70m with  $k = 32$ . An increase in dead latents correlates with a decrease in the auxiliary loss and an increase in the FVU at the last layer. We attribute this to the increased scale of the inputs because the auxiliary loss depends on the MSE (Figure 5). The auxiliary loss is multiplied by its coefficient  $\alpha = 1/32$  in the training loss.

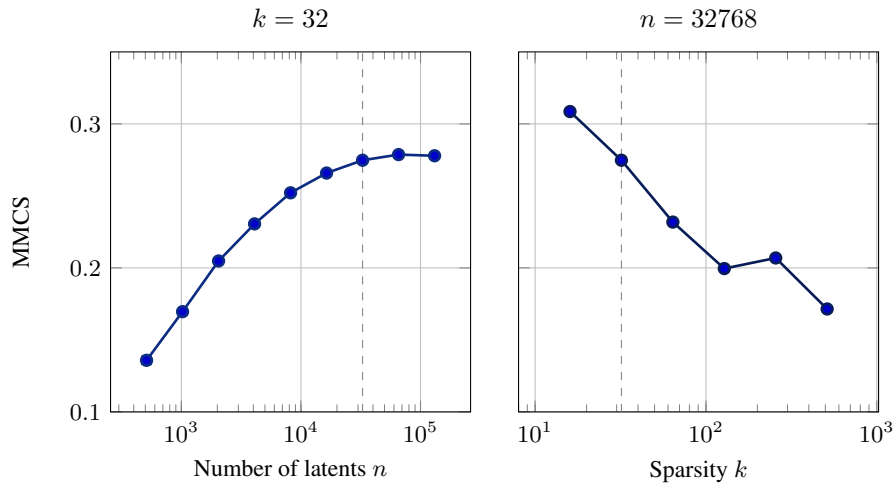


Figure 9: The Mean Max Cosine Similarity for MLSAEs trained on Pythia-70m. The error bars show the standard errors in the mean, but are too small to be visible.

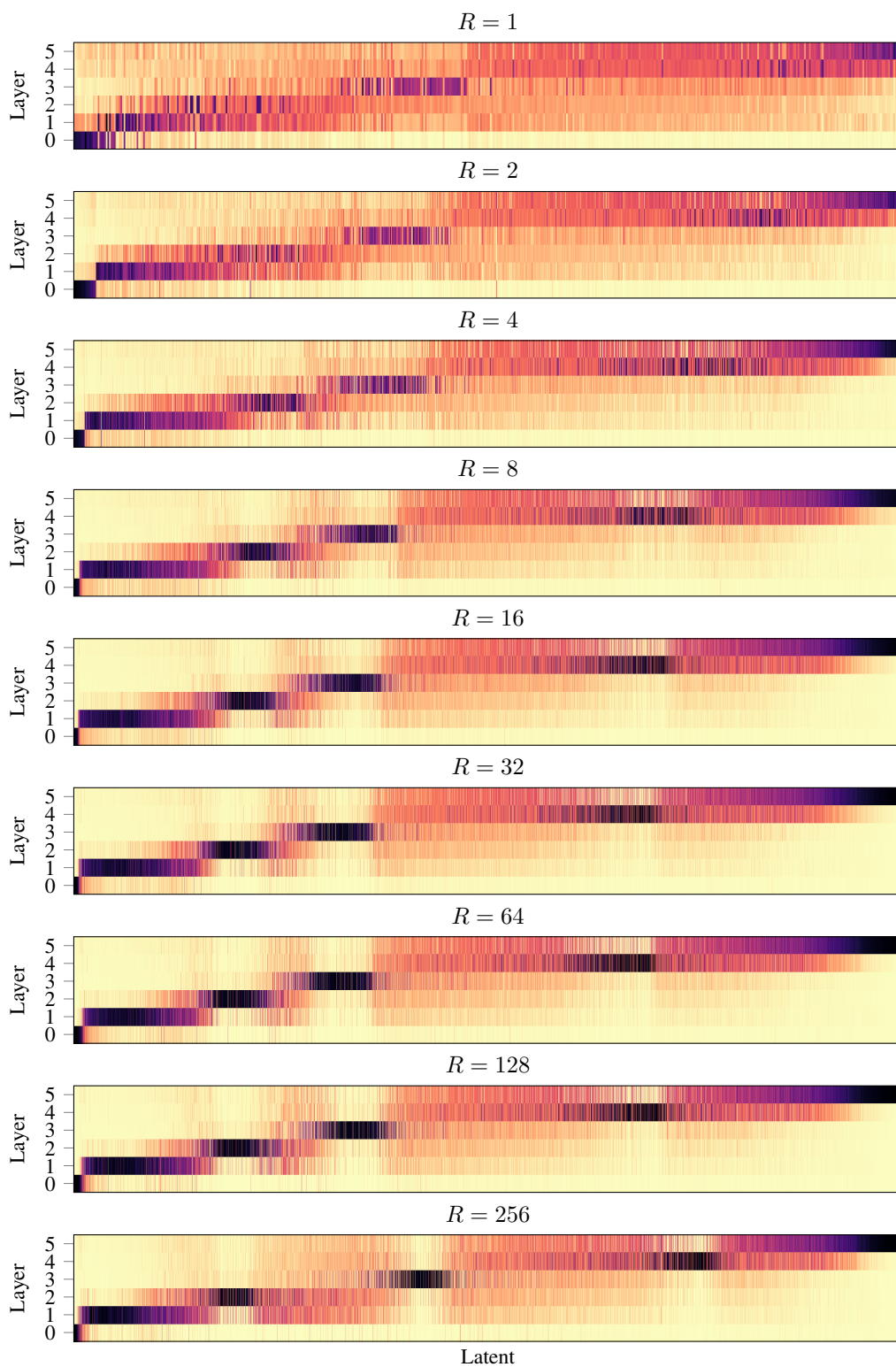


Figure 10: Heatmaps of the distributions of latent activations over layers for MLSAEs trained on Pythia-70m with  $k = 32$  over the entire training dataset. We exclude latents that never activate (0.9% for  $R = 128$  and 1.2% for  $R = 256$ ). We provide further details in Figure 2.

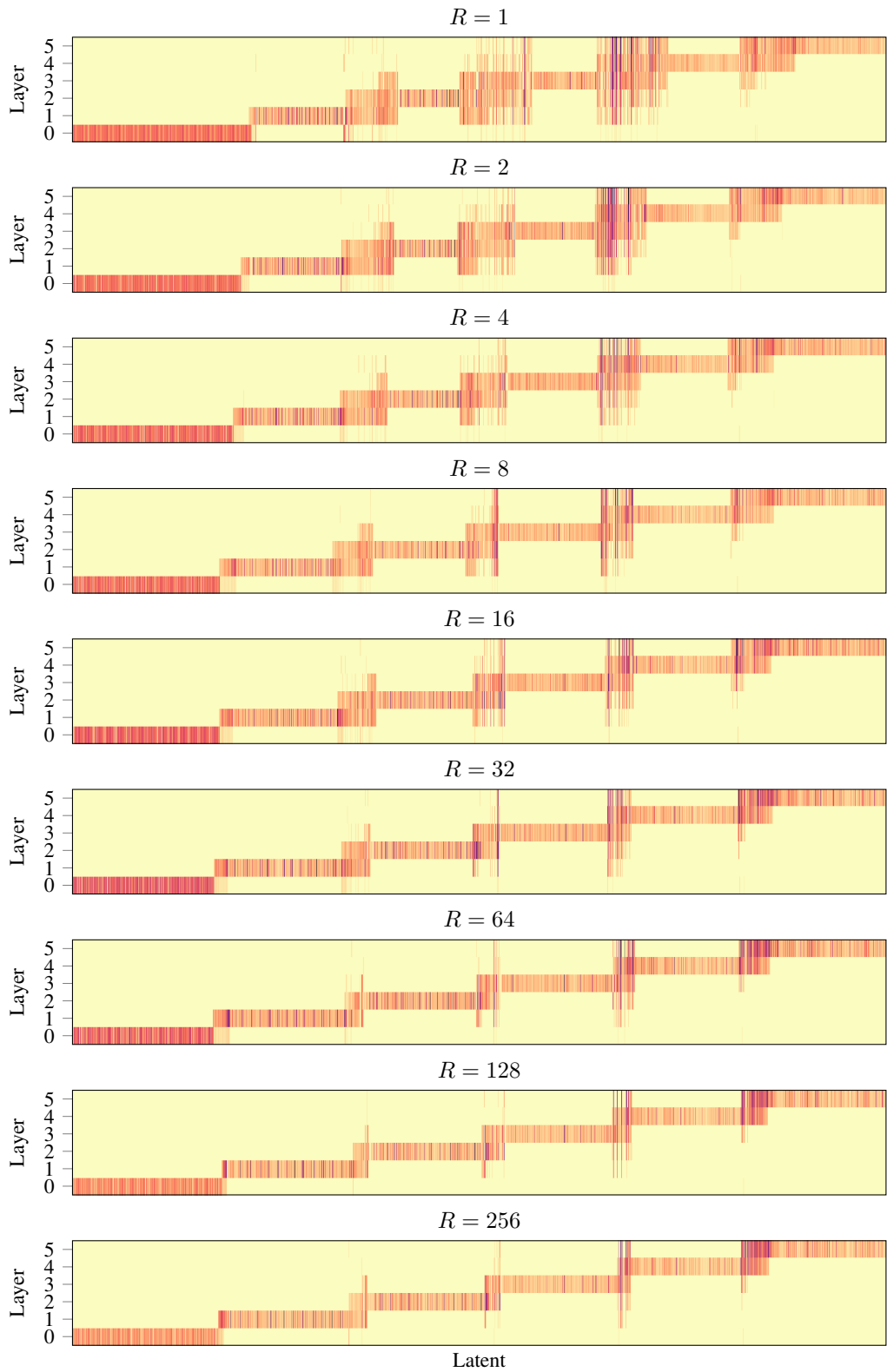
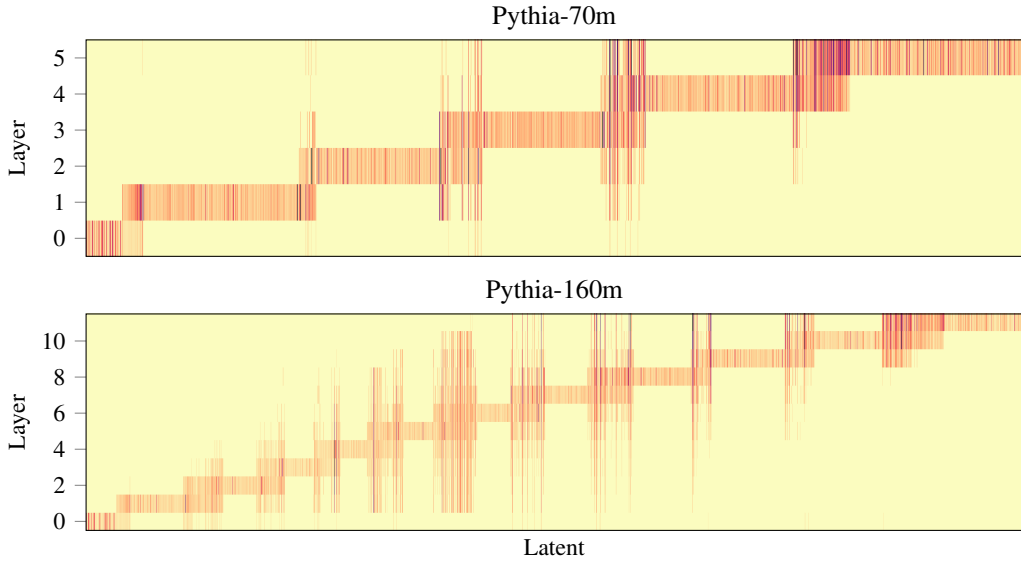
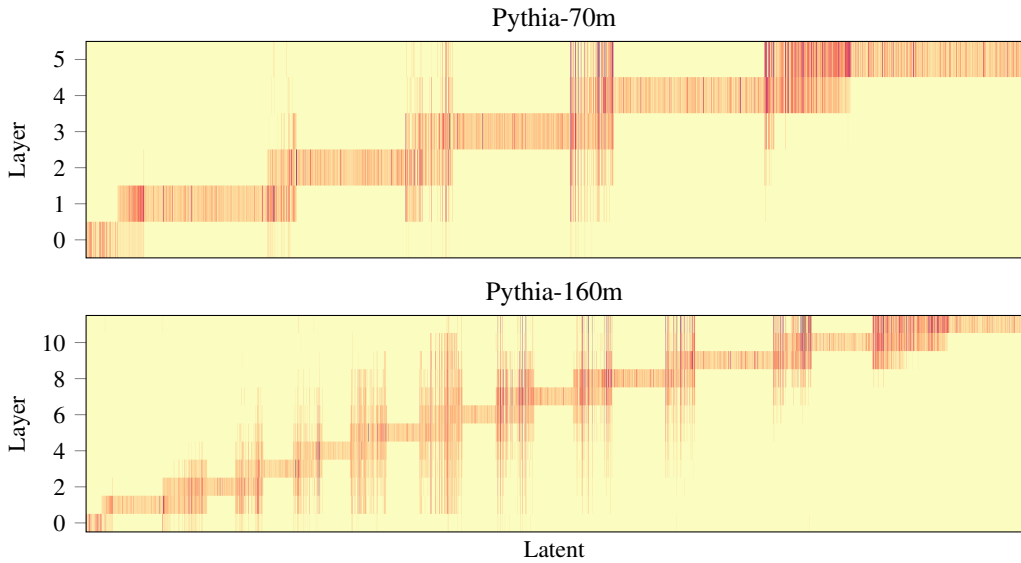


Figure 11: Heatmaps of the maximum latent activations for MLSAEs trained on Pythia-70m with  $k = 32$ , given the prompt “When John and Mary went to the store, John gave” (Wang et al., 2022). We provide further details in Figure 3.



(a) The first example from the validation split of the `machine_learning` subset: “Which of the following guidelines is applicable to initialization of the weight vector in a fully connected neural network.”



(b) The first example from the validation split of the `philosophy` subset: “One of the aims of philosophy is to think critically about whether there are good reasons for adopting our beliefs. Reasons are considered "good reasons" if they are consistent with everyday experience and:”.

Figure 12: Heatmaps of the maximum latent activations of MLSAEs trained on Pythia-70m and 160m with an expansion factor of  $R = 64$  and  $k = 32$ , given prompts from the MMLU dataset (Hendrycks et al., 2021). We provide further details in Figure 3.